

## Thermal Transport in Graphene and Graphene-based Composites

Jiuning Hu<sup>ab</sup>, Wonjun Park<sup>ab</sup>, Xiulin Ruan<sup>cb</sup>, and Yong P. Chen<sup>dba</sup>

<sup>a</sup> School of Electrical and Computer Engineering, Purdue University, West Lafayette, IN 47907, U.S.A.

<sup>b</sup> Birck Nanotechnology Center, Purdue University, West Lafayette, IN 47907, U.S.A.

<sup>c</sup> School of Mechanical Engineering, Purdue University, West Lafayette, IN 47907, U.S.A.

<sup>d</sup> Department of Physics, Purdue University, West Lafayette, IN 47907, U.S.A.

We theoretically and experimentally studied the thermal transport properties in various graphene-based systems. Firstly, we review our previous works of molecular dynamics simulations to study the thermal transport in graphene nanoribbons (GNRs). We also studied negative differential thermal conductance (NDTC) at large temperature biases in GNRs. We extended our study of NDTC in the diffusive limit into general one-dimensional thermal transport and found that NDTC is possible if thermal junctions are introduced. These findings are useful for future applications of controlling heat at nanoscale. Secondly, we describe our experimental work of synthesized graphene-based composites with fillers of reduced graphene oxide and polymers. We used  $3\omega$  method to measure the thermal conductivity and found that the thermal conductivity can be tuned dramatically by the graphene filler concentration. Graphene-based composites are potentially promising as thermal interface materials, which have become increasingly important in modern heat management in many industrial applications.

### Introduction

Graphene has emerged as one of the most attractive materials in recent years and exhibits many unique and excellent properties (1), inviting a broad area of fundamental studies and applications. The measured thermal conductivity of graphene is  $\sim 600 - 5000$  W/m-K (2-6), among the highest value of the existing materials. This attracts intense attention from many fields and opens tremendous possibilities of useful applications such as thermal management. In this paper, firstly, we will review our previous theoretical works on thermal transport in graphene nanoribbons (GNRs) and other related works. Our molecular dynamics simulations presented various properties of GNRs such as chirality dependent thermal conductivity and thermal rectification in asymmetric GNRs. Beyond linear response, we obtained negative differential thermal conductance (NDTC) when the temperature bias is large. We also considered the diffusive thermal transport in general 1D systems and obtained the necessary and sufficient conditions of the existence of NDTC. Our prediction is useful to build practical devices based on NDTC for thermal management. Secondly, we will present our experimental investigations of thermal transport in various graphene-based composites using  $3\omega$  measurement. We find that the

thermal conductivity of composite can be dramatically changed by varying the graphene filling concentrations, which will make graphene composite a potential candidate in the application of heat management such as thermal interface materials.

### Molecular dynamics simulation of thermal transport in GNRs

Molecular dynamics (MD) simulation is useful and predictive to study thermal transport in various structures and compositions of materials. It is particularly convenient for carbon-based systems, since the potential functions needed for the covalent bonding between carbon atoms are well developed during the past two decades (7-9). MD studies using those potentials and numerical recipes can simulate the atomic movement of systems instantaneously and drive the system into either equilibrium or non-equilibrium steady states to study the thermal transport (coefficients) from the fluctuation-dissipation theorem or direct calculations of relevant physical quantities such as the local temperatures and heat current. For classical MD simulation, the computational procedures are in-expensive and highly scalable, which makes it an indispensable tool to study the entire structure/system that may be experimentally produced with modern nanotechnologies.

#### Molecular dynamics simulation procedure

We employed the Brenner potential (9) to simulate the many-body carbon-carbon interactions. The simulation setup and important equations are shown in Fig. 1. In the simulation, the typical GNR consists of 5 parts. The left- and right-most columns of atoms denoted by black squares are position-fixed to eliminate the non-necessary global translation/rotation/folding of the GNR. The atoms denoted by left- and right-pointing atoms are placed in two Nosé-Hoover thermostats (10-11) at two temperatures  $T_L$  and  $T_R$ , respectively. The atoms in the Nosé-Hoover thermostats obey the equation of motion shown in the bottom left box in Fig. 1, where  $p_i$  is the momentum of the  $i$ -th atom,  $F_i$  is the total force acting on the  $i$ -th atom,  $\gamma$  is the Nosé-Hoover dynamic parameter,  $\tau$  is the thermostat relaxation time,  $T(t)$  is the instantaneous temperature at time  $t$  for the group of atoms in left or right thermostat, and  $T_0$  is the desired temperature. The instantaneous temperature is defined in bottom right box where  $N$  is the total number of atoms in the thermostat,  $k_B$  is the Boltzmann constant,  $m$  is the mass of carbon atoms, and the sum is running over all atoms in the thermostat. The atoms denoted by circles in the middle region are free from any thermostat and they obey the Newton's law as shown in the top left box. To calculate the thermal conductivity, we used Fourier's law as shown in the top right box, where  $d$  is the length,  $w$  is the width and  $h$  ( $=0.335$  nm) is the thickness of the GNR. We have applied this MD procedures in our previous studies (12-16) and other details of the simulation can be found there.

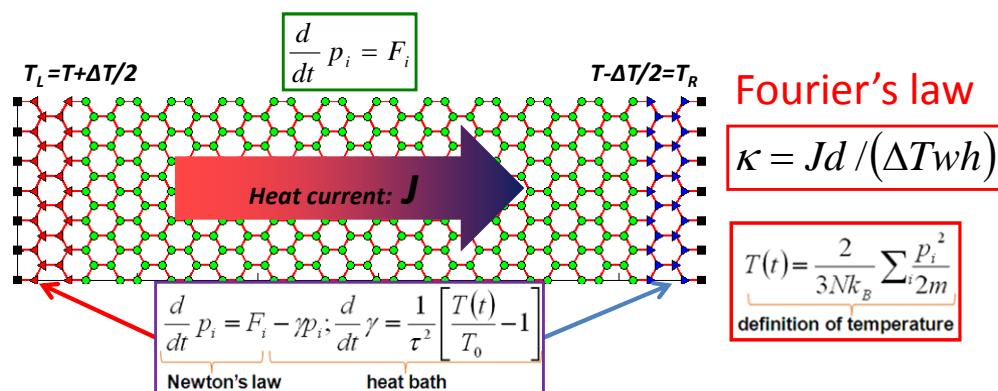


Figure 1. Non-equilibrium molecular dynamics simulation setup and equations for a typical GNR.

### Thermal conductivity and thermal rectification of GNRs

The thermal conductivity of GNRs is calculated according to Fourier's law when the temperature bias is small enough so that the heat current flowing in the system is proportional to the temperature bias. Meanwhile, the temperature bias is selected to be large enough to overcome the intrinsic thermal fluctuation in MD simulations. The thermal conductivity we calculated is  $\sim 1000 - 2000$  W/m-K for typical rectangular GNRs (12). The chirality dependence of thermal conductivity indicates that the thermal conduction is optimal along zigzag edges of GNRs. We list the calculated thermal conductivity of graphene systems from MD simulations and other methods in table I since our work in 2009. We can see that most of these models predicted thermal conductivities of graphene systems of a few hundred to a few thousand W/m-K, while a few models predicted 1 - 2 orders magnitude lower values of thermal conductivity. This large discrepancy exists in the prediction of thermal conductivity, partly due to the choice of intra-atomic potentials, formula for heat currents, calculation schemes, etc.

Table I. A partial list of the simulations of thermal conductivity of graphene systems around room temperature. Non-equilibrium MD: NEMD. Equilibrium MD: EMD. Nonequilibrium Green's function: NEGF. Boltzmann transport equation: BTE.

System	Method	Thermal conductivity (W/m-K)	References
GNRs	NEMD	$\sim 1000 - 2000$	(12)
Graphene	BTE	$\sim 3600$	(17)
GNRs	EMD	$\sim 8000 - 10\,000$	(18)
GNRs	NEGF	$\sim 10 - 20$	(19)
Graphene/GNRs	EMD	$\sim 500 - 2500$	(20)
Narrow GNRs	NEGF	$\sim 1$	(21)
GNRs	NEMD	$\sim 80$	(22)
GNRs	NEMD	$\sim 1600 - 2300$	(23)
GNRs	BTE	$\sim 5000$	(24)
GNRs	NEMD	$\sim 190$	(25)
GNRs	EMD	$\sim 3000$	(26)
GNRs	NEMD	$\sim 50 - 80$	(27)
GNRs	NEMD	$\sim 2400$	(28)
GNRs	EMD	$\sim 800$	(29)

Due to the 2D nature of graphene, it is interesting to study the geometric dependence of thermal transport phenomena when graphene is patterned into various geometries. Of particular interests is the existence of thermal rectification in asymmetric graphene structures that is promising in nano-fabrication patterning (30). Thermal rectification refers to the phenomena that the thermal transport is dependent on the direction of heat flow. In most cases, thermal rectification is studied at forward and backward directions of heat flow. Thermal rectification factor is defined as the relative difference of thermal transport quantities such as thermal conductivities and heat current under same magnitude of heat current in both directions. We predicted that there exists thermal rectification in triangular and trapezoidal GNRs (12-13). Since our work, there are many studies focused on thermal rectification in graphene systems. We list the thermal rectification factor in graphene related systems in Table II.

Table II. A partial list of studies of thermal rectification in graphene related systems around room temperature.

System	Method	Thermal rectification factor	References
Triangular/trapezoidal GNRs	NEMD	~ 10 - 70%	(12-13)
GNRs with asymmetrical strain	NEMD	~ 0 - 75%	(31)
Trapezoidal/T-shaped GNRs	NEMD	~ 100 - 250%	(32)
Asymmetrically defected GNRs	NEMD	~ 30 - 50%	(33)
Asymmetric three-terminal GNRs	NEGF	< 200%	(34)
Graphene-graphane nanoribbon	NEMD	~ 20%	(35)
Graphene Y junctions	NEMD	~ 25 - 45%	(36)
Asymmetric graphene grain boundary	NEMD	~ 70%	(37)
Asymmetric U-shaped GNRs	NEMD	< 120%	(38)
Möbius graphene strip	NEMD	~ 35%	(39)
Three-terminal graphene junctions	NEGF	~ 2%	(40)
Thickness-asymmetrical GNRs	NEMD	~ 20 - 110%	(41)
Partially unzipped carbon nanotubes	NEMD	~ 10 - 180%	(42)

#### NDTC in GNRs and general diffusive 1D systems

In the previous sections, we present the thermal transport properties of graphene related systems in the linear response regime, i.e., the temperature bias applied to the system is small so that the corresponding heat current flow is proportional to the temperature bias. However, as we have shown (14), beyond the linear response regime, the heat current is a non-linear function of the temperature bias. More interestingly, under certain circumstances, if the temperature bias is kept increasing, the heat current flow will start to decrease, exhibiting NDTC in both rectangular and triangular GNRs (15). We have suggested that the mechanism of the existence of NDTC is the competition between temperature dependent thermal conductivity and the temperature bias. Our study of the size dependence of NDTC demonstrates that the magnitude of NDTC decreases as the system size increases.

This motivates us to investigate whether the vanished NDTC at large size is a universal behavior or specific to graphene systems. We assume that for large enough system the thermal transport is diffusive, which allow us to describe the thermal transport using Fourier's law. We showed that NDTC cannot exist when there are no thermal junctions, even when the thermal conductivity has explicitly position and temperature dependence (43). This is a general conclusion, and explains the vanishing behavior of NDTC for long GNRs. However, if there are thermal junctions in the system, NDTC can exist. As in Ref. (43), consider the general 1D system with left and right end at temperatures  $T^L$  and  $T^R$  respectively. The corresponding heat current is denoted by  $q(T^L, T^R)$ . The differential thermal conductance is defined by  $G^L = \partial q / \partial T^L$  and  $G^R = -\partial q / \partial T^R$ . NDTC cannot exist when the temperature bias is smaller than a critical temperature  $T_B$  determined from the details of the system, i.e.,  $G^L$  and  $G^R$  are always positive in the shaded yellow region in Fig. 2. This again demonstrates that the existence of NDTC is a phenomenon beyond the linear response regime. The two contour lines in Fig. 2 are corresponding to heat current  $q$  (black solid curve) and  $q' = q + dq$  (red dashed curve) respectively. We can see that when the contour line has negative slope, we have  $G^L G^R < 0$  and thus NDTC exists. This is a sufficient condition of the existence of NDTC. More details about the necessary and sufficient conditions of the existence of NDTC can be found in Ref. (43). This could potentially lead to building the first practical NDTC device.

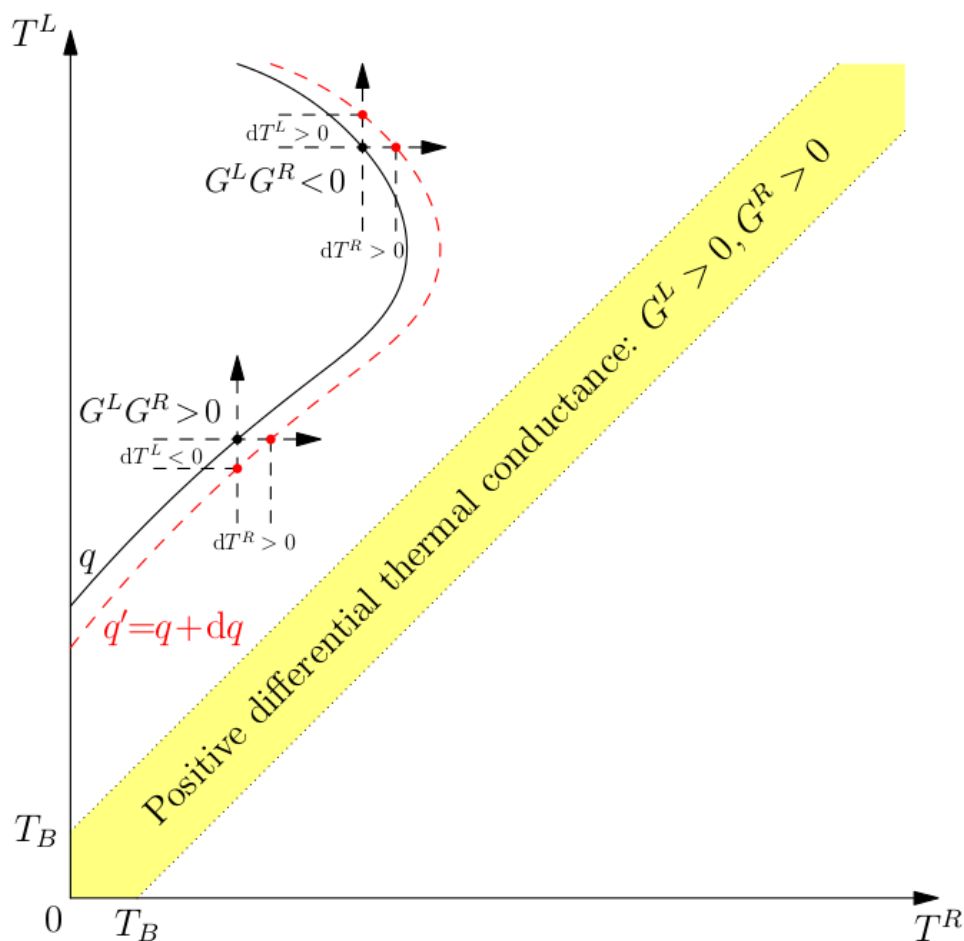


Figure 2. Schematic contour lines of heat current for the existence of NDTC.

## Thermal transport in graphene composites

Graphene composite (GC) materials have drawn much attention recently mainly due to their potential of large scale applications through mass production and abilities to tune their various properties by material engineering (44). GCs exhibit excellent properties, such as extremely low percolation threshold of electrical conductivity (44). Similarly, the thermal properties of GCs can be tuned by controlling graphene concentrations. It has been shown that adding graphene flakes to host materials, such as epoxy (45) and nanostructured phase change materials (46) can dramatically increase the thermal conductivity of the composite materials. It is interesting to investigate the thermal properties of such GCs, and in particular, the graphene concentration dependence of thermal conductivities.

### The synthesis of GCs

The GCs we synthesized are uniform mixture of graphene flakes and polymers of polystyrene (PS) or epoxy. The graphene flakes are massively produced from chemical method of reduced graphene oxide (r-GO). We have synthesized two types of graphene composites.

r-GO/PS composite. Graphite oxide is produced according to Hummers method (47), then functionalized with phenyl isocyanate and finally exfoliated into graphene oxide (GO) in dimethylformamide (DMF) by ultra-sonication. The uniform mixture of GO and PS in dimethylformamide is treated by hydrazine to convert GO to r-GO. The solution is then polymerized using methanol and filtered, followed by drying it in a vacuum oven. The polymerized composite is milled into fine powders and hot pressed into bulk dense composite plate.

r-GO/Epoxy composite. Graphite oxide is exfoliated in deionized water using ultra-sonication followed by the chemical reduction process. It is filtered and dried in vacuum oven. The r-GO powder is then mixed with EPON Resin 862 (Momentive) and EPIKURE W curing agent (Momentive) and the mixture is cured in vacuum oven at 100 °C for 2 hours and at 150 °C for another 2 hours.

The surface of GCs is then polished with fine alumina particles (50nm). Polyvinyl alcohol was spin-coated as an insulating layer (~ 200 nm thick) and the metal line (40 μm wide and 4 mm long) of Cr (20nm)/Au (180nm) is deposited as a heater/sensor for  $3\omega$  measurement.

### Method of $3\omega$ measurement of thermal conductivity

The  $3\omega$  method (48) is employed to measure the thermal conductivity of GCs. During the measurement, first, the temperature coefficient of the metal line is measured for calibration in later data fitting. The sample is then placed in a vacuum stage with pressure typically less than  $10^{-5}$  Torr. All of the measurements are done around room temperature. An electrical bridge is used to cancel the dominant  $1\omega$  signal to increase the  $3\omega$  signal to noise ratio. The  $3\omega$  voltage  $V_{3\omega}$  (amplitude value) is then taken over the frequency range of 10-1000 Hz. To calculate the thermal conductivity,  $V_{3\omega}$  is firstly converted to the thermal impedance  $Z(\omega) = -4V_{3\omega}/(I_{1\omega}V_{1\omega}^2\beta)$  where  $I_{1\omega}$  is the amplitude of the  $1\omega$  current

component flowing in the metal line,  $V_{1\omega}$  is the amplitude of the voltage drop of  $1\omega$  component along the metal line and  $\beta$  is the temperature coefficient of the metal line. Since the thickness of the composite ( $\sim 1$  mm) is much larger than the thermal wave penetration depth in the frequency range of 10 - 1000 Hz, it is safe to approximate the metal line as sitting on a semi-infinite graphene composite, and the thermal impedance can be expressed as

$$Z(\omega) = \frac{1}{\pi L \kappa a^2} \int_0^\infty dl \frac{\sin^2 la}{l^2 \sqrt{l^2 + i2\omega C / \kappa}} \quad [1]$$

where  $L$  is the length of the metal line,  $a$  is the half-width of the metal line,  $C$  is the product of mass density and specific heat capacity of graphene composites, and  $\kappa$  is the thermal conductivity of graphene composites (49). Eq. [1] is used to fit two parameters  $C$  and  $\kappa$ . We benchmark our measurement setup and procedures on glass slide and silicon. The measured thermal impedance is complex, and its in-phase (real part) and out-of-phase (imaginary part) components are separately plotted in Fig.3. We fit the in-phase data to Eq. [1] to obtain  $C$  and  $\kappa$  and then insert these two parameters back to Eq. [1] to calculate the out-of-phase component. As we can see from Fig. 3, the calculated and measured out-of-phase components agree excellently. The measured thermal conductivities for glass slide and silicon are 1.48 W/m-K and 144 W/m-K respectively. They agree well with reported values (50-51) and thus validate our measurement systems. The measurement accuracy is expected even higher for graphene composites since they typically have thermal conductivity around 1 W/m-K.

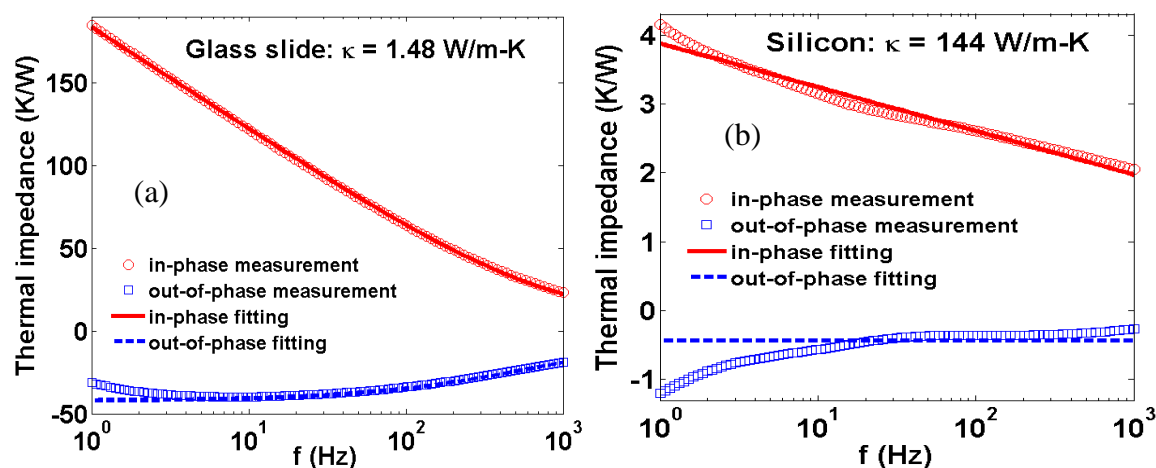


Figure 3. Thermal impedance measurement of (a) glass slides and (b) silicon using  $3\omega$  method.

### Thermal conductivity of graphene composites

The measured thermal conductivity of graphene composites is listed in Table III. The pure polystyrene we measured has a thermal conductivity of 0.157 W/m-K which is very close to the reported value (52-53). The pure epoxy we measured has a thermal conductivity of 0.199 W/m-K which is extremely close to the reported value (54). By adding 5 vol.% of r-GO, the thermal conductivity is increased by 47% and 87% for r-GO/PS and r-GO/epoxy composites respectively. The r-GO/epoxy composite is more

effective to have enhanced thermal conductivity by adding graphene and it may be potentially useful for thermal interfacial material application. A systematic study of thermal transport in GCs with other filling fractions is in progress and will be presented elsewhere (55).

Table III. Measured thermal conductivity of GCs.

Graphene composites	Thermal conductivity $\kappa$ (W/m-K)
0 vol.% r-GO/PS	0.157
5 vol.% r-GO/PS	0.230
0 vol.% r-GO/epoxy	0.199
5 vol.% r-GO/epoxy	0.372

## Conclusions

We have reviewed our theoretical studies of the thermal transport GNRs using classical molecular dynamics simulations. Our predictions include the following aspects. The calculated thermal conductivity of symmetric rectangular GNRs depends on the edge chirality of GNRs and is on the same order of magnitude as the value expected for graphene but with differences likely caused by the finite sizes of GNRs and the choice of numerical procedures. We have demonstrated the thermal rectification effect in asymmetric triangular and trapezoidal GNRs. We have studied the nonlinear thermal transport in GNRs under large temperature biases. We find that in short (6 nm) rectangular GNRs, the NDTC exists in a certain range of applied temperature difference. As the length of the rectangular GNR increases, NDTC gradually weakens. In order to consider the possibility of the existence of NDTC for long GNRs that are believed to work in the diffusive regime, we also study the steady state 1D thermal transport in general diffusive regime. We find that NDTC cannot exist in systems without any abrupt thermal junctions. However, we could have NDTC by introducing temperature dependent thermal contact resistances (TCRs). Our predictions provide a novel approach to realize NDTC through careful thermal contact engineering.

Experimentally, we have synthesized graphene composite using chemically reduced graphene as filling and polystyrene or epoxy as matrix materials. We have prepared samples with different graphene filling concentrations. The measured thermal conductivity is increasing with the filling fraction of graphene. The enhancement can be as high as 87% for 5 vol.% filling for the r-GO/epoxy composite which make it suitable for thermal interfacial material applications.

## Acknowledgments

We acknowledge NRI, CTTC and DTRA for supporting our research.

## References

1. A. H. C. Neto, F. Guinea, N. M. R. Peres, K. S. Novoselov and A. K. Geim, *Rev. Mod. Phys.*, **81**, 109 (2009).
2. A. A. Balandin, S. Ghosh, W. Bao, I. Calizo, D. Teweldebrhan, F. Miao, and C. N. Lau, *Nano Lett.*, **8**, 902 (2008).

3. W. Cai, A. L. Moore, Y. Zhu, X. Li, S. Chen, L. Shi, and R. S. Ruoff, *Nano Lett.*, **10**, 1645 (2010).
4. C. Faugeras, B. Faugeras, M. Orlita, M. Potemski, R. R. Nair, and A. K. Geim, *ACS Nano*, **4**, 1889 (2010).
5. L. A. Jaureguia, Y. Yue, A. N. Sidorov, J. Hu, Q. Yu, G. Lopez, R. Jalilian, D. K. Benjamin, D. A. Delk, W. Wu, Z. Liu, X. Wang, Z. Jiang, X. Ruan, J. Bao, S. S. Pei, and Y. P. Chen, *ECS Trans.*, **28**(5), 73 (2010).
6. J. H. Seol, I. Jo, A. L. Moore, L. Lindsay, Z. H. Aitken, M. T. Pettes, X. Li, Z. Yao, R. Huang, D. Broido, N. Mingo, R. S. Ruoff, and L. Shi, *Science*, **328**, 213 (2010).
7. J. Tersoff, *Phys. Rev. B*, **37**, 6991 (1988).
8. D. W. Brenner, *Phys. Rev. B*, **42**, 9458 (1990).
9. D. W. Brenner, O. A. Shenderova, J. A. Harrison, S. J. Stuart, B. Ni, and S. B. Sinnott, *J. Phys.: Condens. Matter*, **14**, 783 (2002).
10. S. Nosé, *J. Chem. Phys.*, **81**, 511 (1984).
11. W. G. Hoover, *Phys. Rev. A*, **31**, 1695 (1985).
12. J. Hu, X. Ruan and Y. P. Chen, *Nano Lett.*, **9**, 2730 (2009).
13. J. Hu, X. Ruan and Y. P. Chen, *International Journal of Thermophysics*, **33**, 986 (2012)
14. J. Hu, S. Schiffli, A. Vallabhaneni, X. Ruan and Y. P. Chen, *Appl. Phys. Lett.*, **97**, 133107 (2010).
15. J. Hu, Y. Wang, A. Vallabhaneni, X. Ruan, and Y. P. Chen, *Appl. Phys. Lett.*, **99**, 113101 (2011).
16. J. Hu, X. Ruan, Z. Jiang, and Y. P. Chen, *AIP Conference Proceedings*, **1173**(1), 135 (2009).
17. L. Lindsay and D. A. Broido, *Phys. Rev. B*, **82**, 209903 (2010).
18. W. J. Evans, L. Hu and P. Keblinski, *Appl. Phys. Lett.*, **96**, 203112 (2010).
19. Y. Xu, X. Chen, B. Gu and W. Duan, *Appl. Phys. Lett.*, **95**, 233116 (2009).
20. J. Haskins, A. Kinac, C. Sevik, H. Sevinçli, G. Cuniberti and T. Çağın, *ACS Nano*, **5**, 3779 (2011).
21. Z. Tan, J. Wang and C. Gan, *Nano Lett.*, **11**, 214 (2011).
22. N. Wei, L. Xu, H. Wang and J. Zheng, *Nanotechnology*, **22**, 105705 (2011).
23. W. Zhong, M. Zhang, B. Ai and D. Zheng, *Appl. Phys. Lett.*, **98**, 113107 (2011).
24. Z. Aksamija and I. Knezevic, *Appl. Phys. Lett.*, **98**, 141919 (2011).
25. S. Chien, Y. Yang and C. Chen, *Appl. Phys. Lett.*, **98**, 033107 (2011).
26. H. Zhang, G. Lee and K. Cho, *Phys. Rev. B*, **84**, 115460 (2011).
27. T.Y. Ng, J.J. Yeo and Z.S. Liu, *Carbon*, **50**, 4887 (2012).
28. A. Cao, *J. Appl. Phys.*, **111**, 083528 (2012).
29. Y. Wang, B. Qiu and X. Ruan, *Appl. Phys. Lett.*, **101**, 013101 (2012).
30. L. Tapasztó, G. Dobrik, P. Lambin and L. Biró, *Nature Nanotechnology*, **3**, 397 (2008).
31. K. G. S. H. Gunawardana, K. Mullen, J. Hu, Y. P. Chen and X. Ruan, *Phys. Rev. B*, **85**, 245417 (2012).
32. N. Yang, G. Zhang and B. Li, *Appl. Phys. Lett.*, **95**, 033107 (2009).
33. Y. Wang, S. Chen and X. Ruan, *Appl. Phys. Lett.*, **100**, 163101 (2012).
34. T. Ouyang, Y. P. Chen, Y. Xie, X. L. Wei, K. K. Yang, P. Yang and J. X. Zhong, *Phys. Rev. B*, **82**, 245403 (2010).
35. A. Rajabpour, S. M. V. Allaei and F. Kowsary, *Appl. Phys. Lett.*, **99**, 051917 (2011).
36. G. Zhang and H. Zhang, *Nanoscale*, **3**, 4604 (2011).

37. H. Cao, H. Xiang, X. Gong, *Solid State Communications*, **152**, 1807 (2012).
38. J. Cheh and H. Zhao, *J. Stat. Mech.*, **2012**, P06011 (2012).
39. J. W. Jiang, J. S. Wang and B. Li, *EPL*, **89**, 46005 (2010).
40. L. Zhang, J. Wang and B. Li, *Phys. Rev. B*, **81**, 100301(R) (2010).
41. W. Zhong, W. Huang, X. Deng and B. Ai, *Appl. Phys. Lett.*, **99**, 193104 (2011).
42. X. Ni, G. Zhang, B. Li., *J. Phys.: Condens. Matter*, **23**, 215301 (2011).
43. J. Hu and Y. P. Chen, arXiv:1201.3054 (2012).
44. S. Stankovich, D. A. Dikin, G. H. B. Dommett, K. M. Kohlhaas, E. J. Zimney, E. A. Stach, R. D. Piner, S. T. Nguyen and R. S. Ruoff, *Nature*, **442**, 282 (2006).
45. K. M. F. Shahil and A. A. Balandin, *Nano Letters*, **12**, 861 (2012).
46. F. Yavari, H. R. Fard, K. Pashayi, M. A. Rafiee, A. Zamiri, Z. Yu, R. Ozisik, T. Borca-Tasciuc and N. Koratkar, *J. Phy. Chem. C*, **115**, 8753 (2011).
47. W. S. Hummers and R. E. Offeman, *JACS*, **80**, 1339 (1958).
48. D. G. Cahill, *Rev. Sci. Inst.*, **61**, 802 (1990).
49. C. Dames and G. Chen, *Rev. Sci. Inst.*, **76**, 124902 (2005).
50. P. E. Hopkins, B. Kaehr, L. M. Phinney, T. P. Koehler, A. M. Grillet, D. Dunphy, F. Garcia and C. J. Brinker, *J. Heat Transfer*, **133**, 061601 (2011).
51. R. G. Morris and J. G. Hust, *Phys. Rev.*, **124**, 1426 (1961).
52. S. Yu, P. Hing and X. Hu, *Composites Part A: Applied Science and Manufacturing*, **33**, 289 (2002).
53. J. Chiu and P. Fair, *Thermochimica Acta*, **34**, 267 (1979).
54. M. B. Bryning, D. E. Milkie, M. F. Islam, J. M. Kikkawa and A. G. Yodh, *Appl. Phys. Lett.*, **87**, 161909 (2005).
55. W. Park, in preparation (2013).